Space-Charge Layers in All-Solid-State Batteries; Important or Negligible?

de Klerk, Niek; Wagemaker, Marnix

DOI
10.1021/acsaem.8b01141

Publication date
2018

Document Version
Final published version

Published in
ACS Applied Energy Materials

ACS APPLIED ENERGY MATERIALS

Article

Cite This: ACS Appl. Energy Mater. 2018, 1, 5609−5618

www.acsaem.org

Space-Charge Layers in All-Solid-State Batteries; Important or Negligible?

Niek J. J. de Klerk and Marnix Wagemaker*

Department of Radiation Science and Technology, Delft University of Technology, Mekelweg15, 2629JB Delft, The Netherlands

Supporting Information

ABSTRACT: All-solid state batteries have the promise to increase the safety of Li-ion batteries. A prerequisite for high-performance all-solid-state batteries is a high Li-ion conductivity through the solid electrolyte. In recent decades, several solid electrolytes have been developed which have an ionic conductivity comparable to that of common liquid electrolytes. However, fast charging and discharging of all-solid-state batteries remains challenging. This is generally attributed to poor kinetics over the electrode-solid electrolyte interface because of poorly conducting decomposition products, small contact areas, or space-charge layers. To understand and quantify the role of space-charge layers in all-solid-state batteries a simple model is presented which allows to asses the interface capacitance and resistance caused by the space-charge layer. The model is applied to LCO ($LiCoO_2$) and graphite electrodes in contact with an LLZO ($Li_7La_3Zr_2O_{12}$) and LATP ($Li_{1.2}Al_{0.2}Ti_{1.8}(PO_4)_3$) solid electrolyte at several voltages. The predictions demonstrate that the space-charge layer for typical electrode−electrolyte combinations is about a nanometer in thickness, and the consequential resistance for Li-ion transport through the space-charge layer is negligible, except when layers completely depleted of Li-ions are formed in the solid electrolyte. This suggests that space-charge layers have a negligible impact on the performance of all-solid-state batteries.

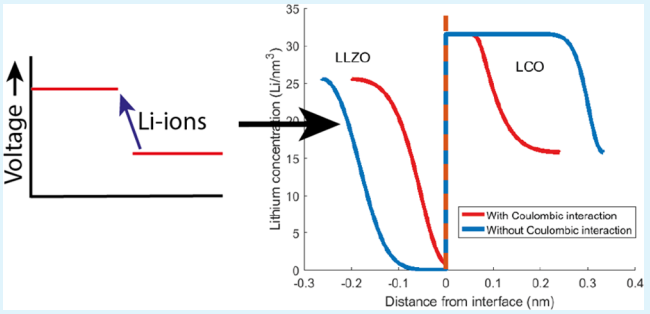

KEYWORDS: *space-charge, all-solid-state batteries, solid state electrolytes, interface, resistance, capacitance*

1. INTRODUCTION

Batteries are becoming increasingly important in modern society by enabling mobile electronic applications, such as smart-phones, laptops, and electric cars. For transport applications batteries are the most sustainable alternative for replacing fossil fuels,[1] but there are concerns whether the safety and energy density of current battery technology is sufficient. All-solid-state batteries (ASSBs) are expected to overcome these concerns[2,3] and even promise to have higher energy densities on the cell level, lower self-discharge rates, and significantly improved safety.

For many years the low ionic conductivity of solid state electrolytes was the main concern for the development of ASSBs, but in recent years many solid state electrolytes with ionic conductivities comparable to those of liquid electrolytes have been discovered.[2] Although the ionic conductivity of solid state electrolytes is comparable to their liquid counterparts nowadays, ASSBs typically show low capacities at high (dis)charge rates,[4,5] which is attributed to the electrode−electrolyte interface. Possible causes for the poor ionic diffusion over the electrode−electrolyte interface are suggested to be[6] a small effective contact area for charge transfer, poorly conducting interphases caused by chemical and electrochemical decomposition, and space-charge effects, which change the conductivity by redistributing the ions near the interface. Ways of increasing the contact area and its effects are being investigated,[4,7,8] and research toward thermodynamic (in)stabilities has resulted in better understanding.[8−11] In comparison, relatively little is known about space-charge effects, and as a consequence the importance of space-charge layers in ASSBs remains unclear.

Space-charge layers in ASSBs have been suggested to be several micrometers in thickness,[12,13] which would cause a large interface resistance. Recent NMR results on Li-ion kinetics show interface resistances of only a few Ω cm^2 over pristine electrode−electrolyte interfaces,[4] and in thin film batteries interface resistances below 10 Ω cm^2 have been reported.[14] Both of which seem incompatible with reports on micrometer thick space-charge layers. Reports indicating that the thickness of the space-charge layer is on the nanometer scale[15,16] seem more compatible with these results, since such a thickness is unlikely to lead to an interface resistance that has a noticeable effect on the performance of ASSBs.

Furthermore, it is being debated if space-charge layers play a role in the beneficial effects of coatings at the electrode-solid electrolyte interface.[16−18] Some authors claim that coating layers reduce the space-charge effect at the interface because of a higher permittivity (dielectric constant) of the material used

Received: July 12, 2018
Accepted: September 25, 2018
Published: September 25, 2018

DOI: 10.1021/acsaem.8b01141
ACS Appl. Energy Mater. 2018, 1, 5609−5618

for the coating.[16,19−21] This is expected to lead to thinner space-charge layers at the electrode-solid electrolyte interface, thus decreasing the interface resistance. Other authors suggest that coatings increase ASSB performance by preventing decomposition of the electrode and electrolyte at the interface. In this case the coating allows Li-ion diffusion, but blocks the diffusion of other atomic species over the interface, thus preventing chemical reactions between the electrode and the solid electrolyte.[22−24]

Since several effects simultaneously play a role at the electrode−electrolyte interface, experimental studies on space-charge effects are challenging. Modeling the space-charge layer is, therefore, an important approach to gain a better understanding of its effects, and models to calculate the lithium concentrations and potentials in solid electrolytes have been developed.[25,26] These models indicate that the space-charge layer is about a nanometer in thickness and that the Li-concentration near the interface can change by 100% in comparison to the bulk concentration. However, these models neglect the Coulomb interactions between charged Li-defects, which are created in the space-charge layer when the Li-ions migrate toward the material with the higher voltage. In AgI, the interaction energy between defects is reported to be 0.68 eV,[27] which represents a significant contribution to the total energy of the material at high defect concentrations. It has been reported that the Coulomb interaction starts to have an impact at a defect concentration of 0.1% already,[28] and the validity of the previous models should therefore be evaluated to comprehend the impact of space-charge layers in all-solid-state batteries.

In the next section, a model for space-charges is presented, which takes the Coulomb interaction between defects into account. The model is used to predict the space-charge at the interface of LCO and graphite electrodes in contact with an LLZO and LATP solid electrolyte at several voltages. Because space-charges are driven by the voltage difference between two materials, which changes during cycling, the space-charges are also determined at different electrode voltages. Using the model the thickness of the space-charge layer at the electrode−electrolyte interfaces is determined, and in addition how much interface resistance this causes. Knowledge of the interface resistance triggered by the space-charge layers provides valuable understanding of its contribution to the internal resistance of ASSBs.

The model is available as Supporting Information in the form of Matlab-code in combination with a short manual. Interested readers can apply the model to the combination of materials they are interested in, provided that the material properties required for the model are known.

2. SPACE-CHARGES

Space-charges have been studied for many years and in numerous materials. They can have beneficial effects, such as increased ionic diffusion in solid−solid dispersions[29−32] and in SEI-layers of liquid electrolytes.[33] But space-charge layers have also been suggested to have detrimental effects on battery performance by increasing the resistance.[16,17,34,35]

A space-charge layer is formed when two materials with different chemical potentials are brought in contact with each other, and the atoms or electrons are unable to migrate to establish local charge neutrality. Near the interface the atoms and electrons are driven toward the material with the lowest chemical potential (highest voltage). But if only one charged species, either electrons or ions, is able to migrate this will create a region in which charge builds up, the so-called space-charge layer.

The insulating nature of solid electrolytes means that the electrons are (practically) unable to conduct, so the amount of electrons transferring over the interface will be negligible. On the other hand, the ionic conduction is several orders of magnitude higher in the solid electrolyte. The potential difference, of several volts, between the electrolyte and electrode will thus drive the mobile ions near the electrolyte-electrode interface toward the material with the lowest chemical potential. This process stops when equilibrium is reached, meaning that the electrochemical potential is constant, which implicates that the attractive chemical potential is balanced by the repulsive electric field build up by accumulation of charge.

The thickness of the space-charge layer and the deviation of the ion concentration from the bulk equilibrium concentration is determined by the properties of the materials which are in contact, including the electric permittivity, ion concentration, and the potential difference between the materials. For a thorough thermodynamic description of the space-charge effect, we refer the reader to the work of Maier and co-workers.[36−38]

Whether the space-charge layer is beneficial or detrimental for ionic conductivity depends on the diffusion mechanism in the solid electrolyte. When Li-vacancies increase the Li-conductivity the space-charge layer is beneficial for Li-conduction over the cathode-solid electrolyte interface,[31] although the magnitude of the effect depends on the cathode material and the cathode voltage. Detrimental effects of space-charges are observed when an increase in Li-vacancies reduces the Li-conduction in the solid electrolyte.[35] Note that space-charges occur under open-circuit conditions, i.e. there is no charge transfer between the anode and cathode. The formation of the space-charge layer thus starts at the moment an electrode and solid electrolyte make contact with each other.

2.1. Electrochemical Potential. To describe the behavior of ions in a battery material the electrochemical potential $(\bar{\mu})$ is used, which consists of the chemical potential (μ) and the electric potential (φ)[39]

$$\bar{\mu} = \mu + ze\varphi \tag{1}$$

where z is the ionic charge and e the elementary charge. In equilibrium the electrochemical potential throughout the material is constant[37,39]

$$\frac{\partial}{\partial x}\bar{\mu}_j = 0 \tag{2}$$

where x is the distance from the interface. Combining eqs 1 and 2 can link the change in electric potential to the change in the chemical potential

$$\Delta\mu_j(x) = -z_j e\Delta\varphi(x) \tag{3}$$

Since the chemical potential depends on the ion concentration, this equation makes it possible to determine the ion concentration as a function of the electric potential.

2.2. Chemical Potential. To describe the chemical potential the solid solution model is used at present, similar to previous models of solid electrolytes[25,26] and electrodes.[40] The Coulomb interactions between charged defects are taken account for as proposed by Maier and co-workers,[28,41] which is required in particular at high defect concentrations. This

DOI: 10.1021/acsaem.8b01141
ACS Appl. Energy Mater. 2018, 1, 5609−5618

results in the following relation between the chemical potential and the ion concentration[27]

$$\mu(\tilde{c}) = \Omega(1 - 2(\tilde{c}_0 + \tilde{c}_d)) + kT \ln\left(\frac{\tilde{c}_0 + \tilde{c}_d}{1 - (\tilde{c}_0 + \tilde{c}_d)}\right) - J\sqrt[3]{|\tilde{c}_d|} \quad (4)$$

where $\tilde{c}$ is the normalized ion concentration (c/c_{max}), $\tilde{c}_0$ is the normalized bulk ion concentration (c_0/c_{max}), and $\tilde{c}_d$ is the normalized ionic defect concentration (negative values for vacancies, positive values for interstitials), Ω is the solid solution parameter, J is the strength of the Coulomb interaction between defects, k is Boltzmann's constant, and T is the temperature in Kelvin.

The strength of the Coulomb interaction can be estimated by the Madelung constants and Madelung energy of a material.[27] Unfortunately, for many materials, the Madelung constants and energies are not reported in the literature. However, it has been shown that the Madelung constant of a material is closely related to its voltage.[42,43] Therefore, the Madelung constants are replaced by the voltages of the material phases, which are filled with ions (V_f) and emptied of ions (V_e). The interaction energy between defects is then obtained using[27]

$$J = \frac{4}{3}\frac{E_M}{\varepsilon}\frac{V_e}{V_f} \quad (5)$$

where E_M is the Madelung energy per Li-equivalent of the structure and ε is the relative permittivity of the material.

2.3. Potential Drop. To determine the concentration profile near the surface and the thickness of the interface layer the potential as a function of the distance must be determined, which requires solving the Poisson equation. Since the electric potential is linked to the chemical potential and ion concentration via eqs 3 and 4, the electric potential can be calculated at different ion concentrations (c_i). By doing this for a range of concentrations the change in distance (Δx) from the bulk with changing concentration can be determined numerically[44]

$$\Delta x = \frac{\varepsilon}{c_{i-1} + \frac{\Delta c}{3}}\left(-E_{i-1} \pm \sqrt{{E_{i-1}}^2 - \frac{2}{\varepsilon}\Delta\varphi\left(c_{i-1} + \frac{\Delta c}{3}\right)}\right) \quad (6)$$

where c_i is the total ion concentration ($c_0 + c_d$) at step i, Δc the concentration difference between step i and $i - 1$, and E_i the electric field at step i. The electric field E_i is calculated by[44]

$$E_i = -\sqrt{\frac{2kT}{\varepsilon}\left(\Delta c - \frac{c_0}{kT}\varphi\right)} \quad (7)$$

Summation over eq 6 results in the concentration (and electric potential) as a function of distance from the bulk. In combination with the boundary conditions presented in the next section this enables determination of the thickness of the space-charge layer at the electrode-solid electrolyte interface.

2.4. Boundary Conditions. To determine what happens when two materials are in contact specific boundary conditions are applied. The first boundary condition is that the created space-charge layer must obey the law of mass conservation. Hence, the number of ions entering one material must be equal to the number of ions that leave the other material

$$\int_{x=0}^{bulk} c_d^{lyte}\,dx = -\int_{x=0}^{bulk} c_d^{trode}\,dx \quad (8)$$

where c_d^{lyte} is the defect concentration in the electrolyte and c_d^{trode} is the defect concentration in the electrode (c_d has a negative value for vacancies and a positive value for interstitials).

Furthermore, the total voltage difference over the interface region must be equal to the voltage difference between the bulk phases of the two materials. This provides the second boundary condition, which states that the total voltage difference over the interface (ΔV_{tot}) must be equal to the combined potential change in the interface region of the electrode (ΔV_{trode}) and electrolyte (ΔV_{lyte})

$$\Delta V_{tot} = \Delta V_{lyte} + \Delta V_{trode} \quad (9)$$

Using the equations and boundary conditions described a 1D-model of the space-charge layer is obtained, under the assumptions that only the ions are mobile, the two materials are chemically stable toward each other, and the presence of a perfect interface contact.

2.5. Space-Charge Resistance and Capacitance. To determine the effect of the space-charge layer on the performance of ASSBs the resistance and capacitance of the space-charge layer are calculated. The capacitance (C) is determined by the number of Li-ions transferred toward the high voltage side divided by the change in voltage of these Li-ions

$$C = \int_{x=0}^{bulk} \frac{c_d(x)}{\Delta V_{tot} - \Delta\varphi(x)}dx \quad (10)$$

To determine the resistance caused by the space-charge layer the large changes in Li-concentration must be taken into account, since this leads to large changes in the lithium diffusivity.[45,46] In LCO[46] the Li-diffusivity (D) shows a minimum at a fractional Li-concentration ($\tilde{c}$) of 0.5, the concentration dependence is thus approximated by

$$D = D^*|\tilde{c} - 0.5| + D_{min} \quad (11)$$

where D^* is the tracer diffusivity and D_{min} is the minimal diffusivity, which is introduced to avoid infinitely small values near $\tilde{c} = 0.5$.

The Li-diffusivity in graphite[45] shows two minima, around $\tilde{c} = \frac{1}{3}$ and $\tilde{c} = \frac{2}{3}$, the concentration dependence is thus approximated by

$$D = D^*\left|\tilde{c} - \frac{1}{3}\right|\left|\tilde{c} - \frac{2}{3}\right| + D_{min} \quad (12)$$

For the solid electrolytes, the concentration dependence of the lithium diffusivity is not reported over a wide concentration range in literature, but a reasonable assumption is that a 50% site-occupancy displays the highest lithium diffusivity.[47] Therefore, the lattice diffusion,[40] showing a maximum diffusivity at $\tilde{c} = 0.5$, is applied for the solid electrolytes

$$D = D^*\tilde{c}(1 - \tilde{c})) \quad (13)$$

The conductivity (σ) of a material can then be calculated using the Nernst−Einstein relation

$$\sigma = \frac{e^2z^2}{kT}cD \quad (14)$$

DOI: 10.1021/acsaem.8b01141
ACS Appl. Energy Mater. 2018, 1, 5609−5618

Table 1. Material Properties Used in the Space-Charge Model

property	LCO	graphite	LATP	LLZO
c_{max} (Li/nm^3)	31.6[48]	16.93[48]	13.06[49]	54.97[50]
c_0 (Li/nm^3)	variable	variable	5.37[49]	25.65[50]
voltage (vs Li/Li$^+$)	3.8−4.4[51]	0.1−0.2[40]	2.5[52]	2.85[53]
ε (relative to ε_0)	12.9[54]	11[55]	15[56]	60[57,58]
Ω (eV)	0.026[59]	0.088[40]	0.0	0.0
E_M (eV/Li)	7.0[a60]	4.5[61]	10.6[b]	10.6[a62]
D^* (cm^2/s)	2×10^{-10} [46]	1×10^{-8} [45]	3×10^{-9} [63]	4×10^{-9} [26]
D_{min} (cm^2/s)	1×10^{-12} [46]	1×10^{-11} [45]		

[a]Formation enthalpy instead of Madelung energy. [b]Formation enthalpy of LLZO (see text).

where c is the total Li-concentration. The conductivity in the space-charge layer changes with concentration, so the resistance in the space-charge layer (R_{sc}) is obtained by

$$R_{sc}A = \int_{x=0}^{bulk} \frac{l}{\sigma(x)} dx \quad (15)$$

where l is the distance through which diffusion occurs, A the surface area, and $\sigma(x)$ the conductivity at x. To determine the effect of the space-charge layer the resistance which would be caused by the same diffusion distance in the bulk material (R_{bulk}) is subtracted from the resistance in the space-charge layer (R_{sc}), resulting in the additional resistance (R) in the all-solid-state battery caused by the space-charge layer

$$R = R_{sc} - R_{bulk} \quad (16)$$

3. RESULTS

Using the model described in the previous section the space-charge layers occurring at the interfaces of a high voltage $LiCoO_2$ electrode (LCO) and a low voltage graphite electrode in contact with the solid electrolytes $Li_7La_3Zr_2O_{12}$ (LLZO) and $Li_{1.2}Al_{0.2}Ti_{1.8}(PO_4)_3$ (LATP) are calculated. The material properties used for the simulations are provided in Table 1, for all the calculations a temperature of 300 K was used.

The voltage of LLZO has been determined by measuring the open circuit potential of an LLZO electrode versus lithium metal.[53] To determine the Coulomb interaction in eq 5 for the solid electrolytes, it was assumed that $V_e = V_f$. A value of 0.0 was chosen for the Ω-parameter based on a previous model for solid electrolytes.[26] To determine the Coulomb interaction between defects the Madelung energy is required, but in literature the Madelung energy is only reported for lithiated graphite. For LCO and LLZO, the formation enthalpy is used as an approximation to the Madelung energy, which appears to be a reasonable approximation since the Madelung energy is the largest contributor to the formation enthalpy in ionic crystals.[43,64] In the case of LATP, the Madelung energy and the formation enthalpy are unavailable, and therefore, the formation enthalpy of LLZO was used as an approximation, making it possible to compare the effects of the other material properties of the two solid electrolytes.

With the parameters shown in Table 1 the Coulomb interaction between defects (J) results in 0.84, 1.09, 0.94, and 0.24 eV for LCO, graphite, LATP and LLZO, respectively.

3.1. Interfaces of Cathode and Solid-Electrolyte Materials. At the positive electrode lithium ions near the interface of the cathode and electrolyte material are driven toward the cathode material by its larger voltage (lower chemical potential), thus reducing the lithium concentration in the solid electrolyte. At higher applied voltages during charging the driving force for Li-ions to move from the solid electrolyte to the cathode material increases, and the declining Li-concentration upon charging will facilitate accommodation of the extra Li-ions in the cathode material.

For the LCO-LLZO interface this increases the spatial extend of the space-charge layer with increasing potential of the LCO, as shown in Figure 1. At an LCO potential of 3.9 V,

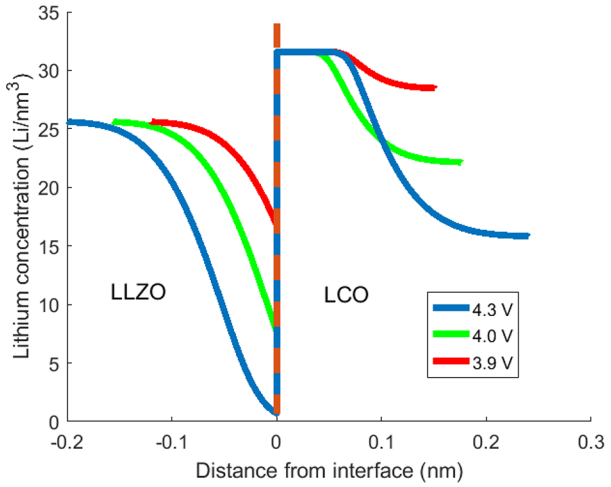

Figure 1. Lithium concentration at the LLZO-LCO interface at different voltages (vs Li/Li$^+$) of LCO: blue = 4.3 V ($Li_{0.5}CoO_2$), green = 4.0 V ($Li_{0.7}CoO_2$), red = 3.9 V ($Li_{0.9}CoO_2$). Where the lines end, the bulk lithium concentration is reached.

the space-charge region is approximately 0.25 nm wide, but at 4.3 V the space-charge region has almost doubled in thickness. The effect on the Li-concentration at the LLZO interface is even more dramatic, at 3.9 V the Li-concentration drops by 35%, while at 4.3 V it decreases by more as 95%.

As shown in Figure 2, the effect of space-charges on the Li-concentration are significantly smaller at the LCO-LATP interface. Although with a thickness of 0.3−0.5 nm the size of the space-charge region is comparable to that at the LCO-LLZO interface, the amount of Li-ions inserted in the LCO is much smaller. The smaller change in Li-concentration in LCO at the LATP interface compared to LCO at the interface of LLZO is caused by the stronger Coulomb interaction between defects in LATP, a consequence of the lower relative permittivity of LATP. This makes it energetically more expensive to remove lithium-ions from LATP, and therefore less lithium ions migrate toward the LCO to compensate for the difference in chemical potential. Although less Li-ions move over the LCO-LATP interface, the lower bulk Li-

DOI: 10.1021/acsaem.8b01141
ACS Appl. Energy Mater. 2018, 1, 5609−5618

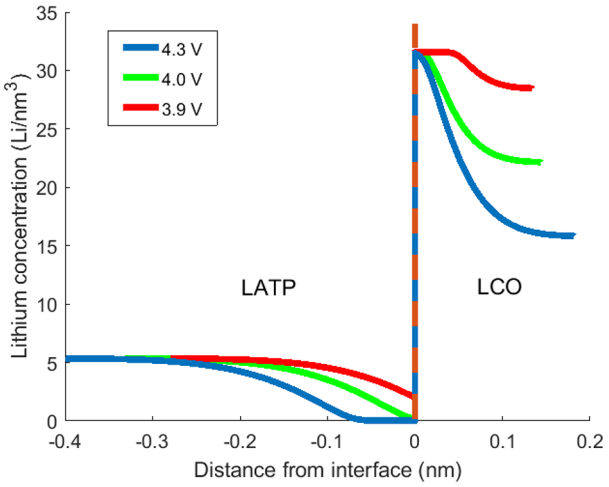

Figure 2. Lithium concentration at the LATP-LCO interface at different voltages of LCO: blue = 4.3 V ($Li_{0.5}CoO_2$), green = 4.0 V ($Li_{0.7}CoO_2$), red = 3.9 V ($Li_{0.9}CoO_2$). Where the lines end the bulk lithium concentration is reached.

concentration in LATP means that a larger percentage of Li-ions is removed, over 60% at 3.9 V and 100% at 4.3 V.

The differences in capacitance of the LCO-LLZO and LCO-LATP interfaces shown in Table 2 reflect the differences in migrated Li-ions. With increasing voltage more Li-ions move into the LCO, thus increasing the capacitance of the space-charge layer. At the LCO-LATP interface this leads to a capacitance of 4−11 $\mu F/cm^2$, while the capacitance at the LLZO interface is between 12 and 49 $\mu F/cm^2$. The calculated capacitances at the interfaces of the LCO and solid electrolytes are comparable to the capacitance reported at the interface of LCO in contact with a liquid electrolyte.[65] Landstorfer et al. have calculated a capacitance of 370.81 $\mu F/cm^2$ at the interface of LLZO with an unspecified cathode material, which is significantly larger compared to the results presented here. This large value can be explained by the fact that the Coulomb interaction was not taken into account and a larger maximum Li-concentration in LLZO was assumed, which both contribute to a higher capacitance.

Table 2. Space-Charge Layer Capacitance and Resistance at the LCO-Solid Electrolyte Interfaces

	LATP		LLZO	
	capacitance ($\mu F/cm^2$)	resistance (Ω cm^2)	capacitance ($\mu F/cm^2$)	resistance (Ω cm^2)
4.3 V	11	17	49	3×10^{-3}
4.0 V	8	2×10^{-2}	29	-2×10^{-4}
3.9 V	4	5×10^{-4}	12	-3×10^{-5}

On the basis of the present model, an increasing potential leads to a rising Li-conductivity in LCO because of an increased Li-concentration and an increased Li-diffusivity. In both solid electrolytes the Li-conductivity decreases, because of a lower Li-concentration and a decreasing Li-diffusivity. At the LCO−LLZO interface, the increase in Li-conductivity through LCO is larger than the decrease in Li-conductivity through the LLZO at 3.9 and 4.0 V, and consequentially the space-charge layer decreases the resistance for Li-ion transport over the interface. When increasing the LCO voltage to 4.3 V the LLZO becomes almost depleted of Li-ions, which leads to an increased resistance over the interface, as shown in Table 2.

At the LCO−LATP interface, the removal of Li-ions from LATP causes larger problems, reflected in the orders of magnitude rise in interface resistance upon increasing the voltage. At 3.9 V the resistance is small, but at 4.0 V the Li-concentration drops significantly, raising the resistance by 2 orders of magnitude. At 4.3 V a Li-depleted layer of 1 Å is formed, in which the Li-conductivity is negligible, and as a result a further increase in the space-charge resistance is observed. However, the resistance of 17 Ω cm^2 reported in Table 2 is doubtful, because it quadratically depends on the lower limit of the Li-concentration allowed in the model via eqs 13 and 14, which is (arbitrarily) set at 0.015 Li/nm^3. [Defining a lower limit for the Li-concentration is necessary because a Li-concentration of zero would cause the resistance to reach an infinite value, which seems unrealistic over distances below a few Ångströms.] Currently, it is unknown which value is realistic for the lower limit for the Li-concentration in LATP, and it could be that a value of 0.15 Li/nm^3 is a more realistic limit, which would reduce the space-charge resistance to 0.3 Ω cm^2, but determining the lower limit of the Li-concentration will require a thorough experimental investigation. In addition, the depletion of Li-ions at the interface may induce local structural changes that have additional consequences on the resistance, not taken into account here.

However, this example does show an advantage of solid electrolytes with high Li-ion concentration, such as LLZO. Although more Li-ions are removed from LLZO than from LATP, the high Li-concentration prevents the formation of a layer depleted of Li-ions, thus leading to a smaller interface resistance due to the space-charge layer.

3.2. Interfaces of Anode and Solid-Electrolyte Materials. At the negative electrode Li-ions near the interface of the electrolyte and the anode material are driven toward the higher Li-voltage (lower chemical potential) of the solid electrolyte. When graphite is in contact with LLZO this leads to a space-charge region in graphite where lithium is completely depleted, while there is a significant increase of Li-ions in the LLZO, as shown in Figure 3.

The thickness of the space-charge layer strongly depends on the voltage applied to the graphite, being approximately 0.4 nm at 0.1 V, increasing to approximately 1 nm. when graphite is at 0.2 V. Even though less Li-ions transfer toward the LLZO at 0.2 V as compared to 0.1 V, a more extensive space-charge layer is formed due to the lower Li-concentration in the graphite bulk.

In Figure 4, it is shown that at the LATP-graphite interface the thickness of the space-charge layer is smaller compared to the LLZO-graphite interface. The lower maximum Li concentration in LATP in combination with its lower permittivity, compared to LLZO, makes it energetically more expensive to change the Li-concentration in LATP, leading to a smaller space-charge layer in the graphite.

The larger Coulomb interaction in LATP in combination with the small change in graphite voltage causes the amount of Li-ions transferring over the interface to be almost equal in all three cases, as demonstrated by the nearly overlapping Li-concentration profiles in Figure 4. In the graphite, the space-charge layer changes considerably with voltage because of the large changes in bulk Li-concentration with voltage. When graphite is at 0.1 V, the Li-concentration is large and Li-ions

DOI: 10.1021/acsaem.8b01141
ACS Appl. Energy Mater. 2018, 1, 5609−5618

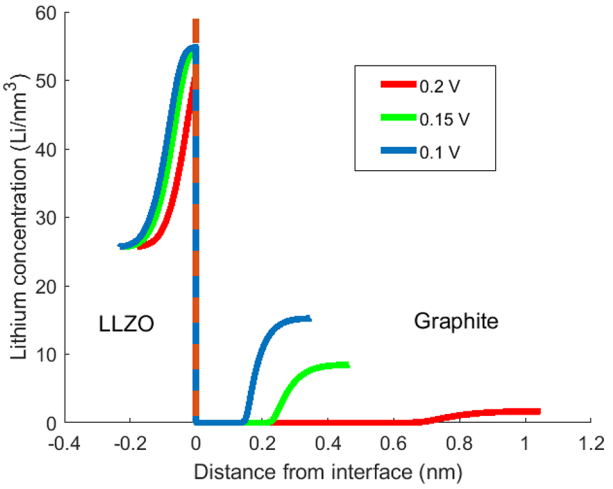

Figure 3. Lithium concentration at the LLZO-graphite interface at different voltages for graphite: blue = 0.1 V ($Li_{0.9}C_6$), green = 0.15 V ($Li_{0.5}C_6$), and red = 0.2 V ($Li_{0.1}C_6$). Where the lines end, the bulk lithium concentration is reached.

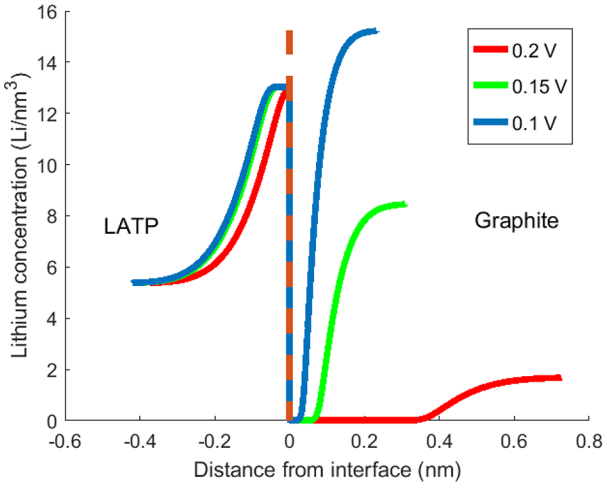

Figure 4. Lithium concentration at the LATP-graphite interface at different voltages for graphite: blue = 0.1 V ($Li_{0.9}C_6$), green = 0.15 V ($Li_{0.5}C_6$), and red = 0.2 V ($Li_{0.1}C_6$). Where the lines end, the bulk lithium concentration is reached.

can easily be extracted, leading to a space-charge layer of 0.4 nm. At higher voltages the Li-concentration in graphite is much lower, and extraction of the same amount of Li-ions leads to a thicker space-charge layer, growing to 0.8 nm when the graphite is at 0.2 V.

In Table 3 the interface capacitances and resistances at the graphite interfaces are shown. In both cases the capacitance increases upon lowering the graphite voltage, because the voltage difference increases, it thus becomes more favorable for Li-ions to migrate toward the solid electrolyte.

Table 3. Space-Charge Layer Capacitance and Resistance at the Graphite-Solid Electrolyte Interfaces

	LATP		LLZO	
	capacitance ($\mu F/cm^2$)	resistance ($\times 10^{-2}\ \Omega\ cm^2$)	capacitance ($\mu F/cm^2$)	resistance ($\times 10^{-2}\ \Omega\ cm^2$)
0.2 V	8	15	9	29
0.15 V	11	4	16	10
0.1 V	12	2	19	6

In all the presented cases the interface resistance is in the order of $10^{-1}\ \Omega\ cm^2$, even though there is always a Li-depleted layer present in the graphite. Although the resistance shows a significant increase when the thickness of the Li-depletion layer increases, in comparison to the Li-depleted layer at LATP–LLZO interface, it has a small effect. This can be explained by the high Li-diffusivity in graphite at low Li-concentrations (eq 12), while the Li-diffusivity drops dramatically in the solid electrolytes at low Li-concentrations (eq 13). As a result the formation of a layer depleted of Li-ions leads to a large interface resistance in LATP, while in graphite the interface resistance remains small. This shows that the resistance caused by space-charge layers strongly depends on the diffusion mechanism, as has been shown experimentally.[31,35]

3.3. Impact of Coulomb Interaction. As discussed, the high defect concentrations in the space-charge layer of ASSBs implies that the Coulomb interaction between defects must be taken into account. To demonstrate the impact of the Coulomb interaction Li-concentration profiles with and without taking the Coulomb interaction into account are shown in Figure 5 for the LCO–LLZO interface at 4.3 V.

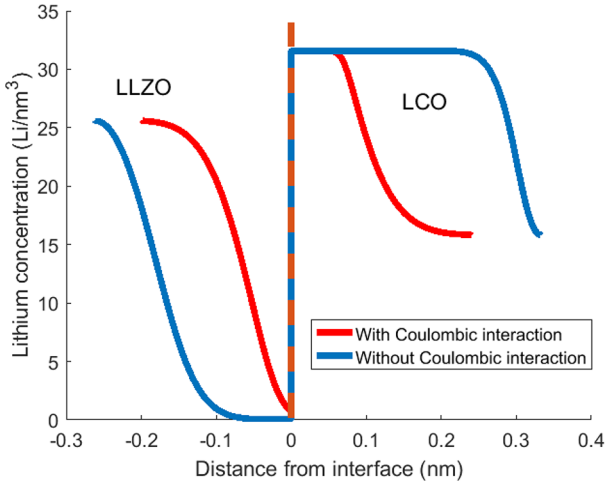

Figure 5. Lithium concentration at the LCO–LLZO interface at 4.3 V with and without Coulomb interactions. Where the lines end the bulk lithium concentration is reached.

Without the Coulomb interaction a steeper and larger change in lithium concentration is predicted, similar to the results of previous models.[25,26] This results in a layer which is completely depleted of Li-ions in the solid electrolyte, a thicker space-charge layer in the LCO, and a larger region in which the maximum lithium concentration is reached.

By neglecting the Coulomb interaction between Li-defects the thickness of the interface layer is almost doubled. In comparison to the results with the Coulomb interaction in Table 2 the interface capacitance increases almost 2-fold to 90 $\mu F/cm^2$, and the interface resistance increases by 2 orders of magnitude to 2 $\Omega\ cm^2$, caused by the low Li-conductivity in the LLZO layer depleted of lithium ions. Neglecting the Coulomb interaction thus has a significant impact on the space-charge layer and its properties, and this demonstrates that the Coulomb interactions between Li-defects cannot be neglected when describing space-charge layers and their effects in ASSBs.

DOI: 10.1021/acsaem.8b01141
ACS Appl. Energy Mater. 2018, 1, 5609–5618

4. DISCUSSION

The presented space-charge model for electrode-solid electrolyte interfaces in ASSBs indicates that the space-charge layer has a thickness in the order of one nanometer, consistent with previous models[25,26] and experiments.[15,16] The resistance, capacitance, and thickness of the space-charge layer are shown to strongly depend on the electrode-solid electrolyte combination and electrode voltage. Taking the Coulomb interaction between defects into account is shown to have a significant effect. It severely reduces the amount of Li-defects formed in the space-charge layer, which in turn leads to a smaller interface capacitance. Comparing the calculations with and without the Coulomb interaction shows that it also has a large effect on the calculated interface resistance.

It should be realized that the current approach has a number of uncertainties. First of all, the Coulomb interaction energy term used here is based on the lattice energy of the crystal times the average distance between Li-defects, giving only a rough approximation of the interactions between charged defects. At high defect concentrations, this approach might also break down when other effects, such as the transfer of electrons over the interface to reduce the Coulomb repulsion, might become more favorable as further increasing the ionic defect concentration.

Furthermore, a simple relation between ionic diffusion and ion concentration (eq 13) was used to calculate the resistance. As shown by Kozinsky et al.[66] the ionic conduction in a solid electrolyte can strongly vary with ion concentration, which influences the resistance over the space-charge layer. Implementing more complex equations to describe the ionic diffusion with changing ion concentration might therefore be necessary to improve the description of the space-charge resistance.

The space-charge model indicates that the Li-concentration in the solid electrolyte can change by 100% at the interface. With such large changes in Li-concentration, it is unlikely that the solid electrolyte retains its original structure and properties. On the other hand, the model suggests that the changes in Li-concentration only occur in the first few atomic layers at the interface, whose structure may be stabilized by the underlying bulk crystal. In addition, the permittivity of the materials will depend on the Li-concentration, which has not been accounted for. Nevertheless, we believe that the presently used approximations allow a prediction that results in space-charge layer properties in the correct order of magnitude.

A comparison between experimental results[4,14] and the model shows large differences in the interface resistance for most cases. Although the LCO-LATP interface at 4.3 V shows a similar interface resistance compared to experiments, in the other cases the differences are most likely caused by the approximation of a perfect and stable interface in the model, which is unlikely to hold for real interfaces.

At the moment electrode and solid electrolyte are brought into contact the high ionic conductivity will cause a transfer of ions over the interface within seconds. This is likely to cause a topotactic phase transition, for which indications have been found experimentally.[11] This will be the starting point of solid electrolyte decomposition, although it is unlikely that the phase formed via the topotactic transition is the thermodynamically most stable phase. More stable phases are likely to form,[11] and even though their growth is kinetically limited[67] experiments have been able to observe these phases grow within a day.[68,69] Extrapolation of the decomposition rate for $Li_{10}GeP_2S_{12}$ (LGPS) shows an expected thickness of the decomposition layer of 370 nm after one year.[68] But this is without considering the effects of cycling the battery, which will lead to further growth of the decomposition layer.[70] In this decomposition layer different phases with differing potentials can occur, thus explaining experimental observations of potential drops at the interface spread out over roughly a micrometer.[12,13] Especially considering the results of the model presented here, the potential drop over the decomposition layer seems to be a more plausible explanation of the experimental observations than a space-charge layer of a micrometer.

The current results also shed light on the effect of coatings at the electrode−electrolyte interfaces. Since the space-charge layers are on the scale of a nanometer, it is unlikely that they improve battery performance by reducing space-charge effects, as has been suggested,[16,19−21] although space-charge layers can become smaller when applying coatings.[71] Instead, the prediction that space-charge layers are small in extend supports the suggestion that coatings improve the performance of ASSBs by preventing interface decomposition of the electrode and electrolyte,[22−24] which underlines that creating a stable electrode−electrolyte interface is essential for creating high-rate ASSBs.

The formation of decomposition products on the electrode−electrolyte interface changes the properties of the materials on the interfaces, new phases might be formed, and the presented space-charge model breaks down. Incorporating the effects of the instability at the interfaces requires the determination of all the relevant parameters for the newly formed phases, which may be an important next step for modeling specific electrode-solid electrolyte interfaces when sufficient data is available.

The nanometer scale of space-charge layers implicates that these will only form when the electrode and solid electrolyte are in contact with each other on the atomic scale, which is essential for charge-transfer over the interface. The space-charge capacitance can thus be used as a measure for the amount of contact area between solid electrolyte and electrode on the atomic scale, which is an important parameter for increasing the performance for ASSB's.

Here, we have shown results for a number of electrode and solid electrolyte combinations, but we have not studied the important class of sulfide solid electrolytes. Since the ion concentration, potential, and dielectric constant are not vastly different between oxide and sulfide solid electrolytes, we expect space-charge layers in the order of a nanometer. But the effects caused by the space-charge layer could be quite different, for example if thick Li-depleted layers cause a large resistance over the space-charge layer. Applying the model to other electrode and solid electrolyte materials would, therefore, be an interesting path for future research.

5. CONCLUSION

The space-charge effect in all-solid-state-batteries is shown to lead to space-charge layers with a thickness in the nanometer regime, causing resistances below one Ω cm^2 at the interfaces investigated, thus having a negligible effect on the performance of ASSBs. A significant increase to the interface resistance is only expected to occur when the solid electrolyte becomes completely depleted of Li-ions in the space-charge layer.

These results suggest that space-charge layers do not stand in the way of high-rate all-solid-state batteries. Instead

DOI: 10.1021/acsaem.8b01141
ACS Appl. Energy Mater. 2018, 1, 5609−5618

formation of poorly conducting decomposition products, as well as small contact areas are expected to induce the large interface resistances observed experimentally.

Furthermore, the Li-concentration in the space-charge layer can change by 100%, although it strongly depends on the combination of materials and the electrode voltage. Taking Coulomb interactions between charged defects into account is shown to have a large impact and, therefore, appears to be essential for a correct description of space-charge layers and their effects in ASSBs.

■ ASSOCIATED CONTENT

Supporting Information

The Supporting Information is available free of charge on the ACS Publications website at DOI: 10.1021/acsaem.8b01141.

Matlab code of the model in combination with a short manual on how to apply the code to model space-charge layers in other materials (ZIP)

■ AUTHOR INFORMATION

Corresponding Author

*E-mail: m.wagemaker@tudelft.nl.

ORCID

Niek J. J. de Klerk: 0000-0002-5100-4883

Marnix Wagemaker: 0000-0003-3851-1044

Notes

The authors declare no competing financial interest.

■ ACKNOWLEDGMENTS

Financial support from the Advanced Dutch Energy Materials (ADEM) program of the Dutch Ministry of Economic Affairs, Agriculture and Innovation is gratefully acknowledged. The research leading to these results has received funding from the European Research Council under the European Union's Seventh Framework Programme (FP/2007-2013)/ERC Grant Agreement nr. [307161] of M.W. The authors would like to thank Hylke Donker and the TCM group at the Radboud University for providing N.K. with a working spot in Nijmegen.

■ REFERENCES

(1) Bauer, C.; Hofer, J.; Althaus, H.-J.; Del Duce, A.; Simons, A. The Environmental Performance of Current and Future Passenger Vehicles: Life Cycle Assessment based on a Novel Scenario Analysis Framework. *Appl. Energy* **2015**, *157*, 871−883.

(2) Lotsch, B. V.; Maier, J. Relevance of Solid Electrolytes for Lithium-Based Batteries: A Realistic View. *J. Electroceram.* **2017**, *38*, 128−141.

(3) Placke, T.; Kloepsch, R.; Dühnen, S.; Winter, M. Lithium Ion, Lithium Metal, and Alternative Rechargeable Battery Technologies: the Odyssey for High Energy Density. *J. Solid State Electrochem.* **2017**, *21*, 1939−1964.

(4) Yu, C.; Ganapathy, S.; Eck, E.; Wang, H.; Basak, S.; Li, Z.; Wagemaker, M. Accessing the Bottleneck in All-Solid State Batteries, Lithium-Ion Transport over the Solid-Electrolyte-Electrode Interface. *Nat. Commun.* **2017**, *8*, 1086.

(5) Takada, K. Solid Electrolytes and Solid-State Batteries. *AIP Conf. Proc.* **2015**, *1765*, No. 020008.

(6) Luntz, A. C.; Voss, J.; Reuter, K. Interfacial Challenges in Solid-State Li Ion Batteries. *J. Phys. Chem. Lett.* **2015**, *6*, 4599−4604.

(7) Tian, H.-K.; Qi, Y. Simulation of the Effect of Contact Area Loss in All-Solid-State Li-Ion Batteries. *J. Electrochem. Soc.* **2017**, *164*, E3512−E3521.

(8) Kim, J. G.; Son, B.; Mukherjee, S.; Schuppert, N.; Bates, A.; Kwon, O.; Choi, M. J.; Chung, H. Y.; Park, S. A Review of Lithium and Non-Lithium Based Solid State Batteries. *J. Power Sources* **2015**, *282*, 299−322.

(9) Zhu, Y.; He, X.; Mo, Y. Origin of Outstanding Stability in the Lithium Solid Electrolyte Materials: Insights from Thermodynamic Analyses Based on First-Principles Calculations. *ACS Appl. Mater. Interfaces* **2015**, *7*, 23685−23693.

(10) Auvergniot, J.; Cassel, A.; Ledeuil, J.-B.; Viallet, V.; Seznec, V.; Dedryvere, R. Interface Stability of Argyrodite Li_6PS_5Cl toward $LiCoO_2$, $LiNi_{1/3}Co_{1/3}Mn_{1/3}O_2$, and $LiMn_2O_4$ in Bulk All-Solid-State Batteries. *Chem. Mater.* **2017**, *29*, 3883−3890.

(11) Tian, Y.; Shi, T.; Richards, W. D.; Li, J.; Kim, J. C.; Bo, S.-H.; Ceder, G. Compatibility Issues between Electrodes and Electrolytes in Solid-State Batteries. *Energy Environ. Sci.* **2017**, *10*, 1150−1166.

(12) Yamamoto, K.; Iriyama, Y.; Asaka, T.; Hirayama, T.; Fujita, H.; Fisher, C. A.; Nonaka, K.; Sugita, Y.; Ogumi, Z. Dynamic Visualization of the Electric Potential in an All-Solid-State Rechargeable Lithium Battery. *Angew. Chem., Int. Ed.* **2010**, *49*, 4414−4417.

(13) Masuda, H.; Ishida, N.; Ogata, Y.; Ito, D.; Fujita, D. Internal Potential Mapping of Charged Solid-State-Lithium Ion Batteries using In Situ Kelvin Probe Force Microscopy. *Nanoscale* **2017**, *9*, 893−898.

(14) Haruta, M.; Shiraki, S.; Suzuki, T.; Kumatani, A.; Ohsawa, T.; Takagi, Y.; Shimizu, R.; Hitosugi, T. Negligible Negative Space-Charge Layer Effects at Oxide-Electrolyte/Electrode Interfaces of Thin-Film Batteries. *Nano Lett.* **2015**, *15*, 1498−1502.

(15) Aizawa, Y.; Yamamoto, K.; Sato, T.; Murata, H.; Yoshida, R.; Fisher, C. A. J.; Kato, T.; Iriyama, Y.; Hirayama, T. In Situ Electron Holography of Electric Potentials Inside a Solid-State Electrolyte: Effect of Electric-Field Leakage. *Ultramicroscopy* **2017**, *178*, 20−26.

(16) Takada, K.; Ohta, N.; Zhang, L.; Xu, X.; Hang, B. T.; Ohnishi, T.; Osada, M.; Sasaki, T. Interfacial Phenomena in Solid-State Lithium Battery with Sulfide Solid Electrolyte. *Solid State Ionics* **2012**, *225*, 594−597.

(17) Takada, K. Progress and Prospective of Solid-State Lithium Batteries. *Acta Mater.* **2013**, *61*, 759−770.

(18) Takada, K.; Ohta, N.; Tateyama, Y. Recent Progress in Interfacial Nanoarchitectonics in Solid-State Batteries. *J. Inorg. Organomet. Polym. Mater.* **2015**, *25*, 205−213.

(19) Okumura, T.; Nakatsutsumi, T.; Ina, T.; Orikasa, Y.; Arai, H.; Fukutsuka, T.; Iriyama, Y.; Uruga, T.; Tanida, H.; Uchimoto, Y.; Ogumi, Z. Depth-Resolved X-ray Absorption Spectroscopic Study on Nanoscale Observation of the Electrode−Solid Electrolyte Interface for All Solid State Lithium Ion Batteries. *J. Mater. Chem.* **2011**, *21*, 10051.

(20) Wu, B.; Wang, S.; Evans Iv, W. J.; Deng, D. Z.; Yang, J.; Xiao, J. Interfacial Behaviours between Lithium Ion Conductors and Electrode Materials in Various Battery Systems. *J. Mater. Chem. A* **2016**, *4*, 15266−15280.

(21) Yada, C.; Lee, C. E.; Laughman, D.; Hannah, L.; Iba, H.; Hayden, B. E. A High-Throughput Approach Developing Lithium-Niobium-Tantalum Oxides as Electrolyte/Cathode Interlayers for High-Voltage All-Solid-State Lithium Batteries. *J. Electrochem. Soc.* **2015**, *162*, A722−A726.

(22) Sakuda, A.; Hayashi, A.; Tatsumisago, M. Interfacial Observation between $LiCoO_2$ Electrode and Li_2S-P_2S_5 Solid Electrolytes of All-Solid-State Lithium Secondary Batteries Using Transmission Electron Microscopy. *Chem. Mater.* **2010**, *22*, 949−956.

(23) Ohtomo, T.; Hayashi, A.; Tatsumisago, M.; Tsuchida, Y.; Hama, S.; Kawamoto, K. All-Solid-State Lithium Secondary Batteries using the $75Li_2S$ - $25P_2S_5$ Glass and the $70Li_2S$ - $30P_2S_5$ Glass-Ceramic as Solid Electrolytes. *J. Power Sources* **2013**, *233*, 231−235.

(24) Takahashi, K.; Hattori, K.; Yamazaki, T.; Takada, K.; Matsuo, M.; Orimo, S.; Maekawa, H.; Takamura, H. All-Solid-State Lithium Battery with $LiBH_4$ Solid Electrolyte. *J. Power Sources* **2013**, *226*, 61−64.

DOI: 10.1021/acsaem.8b01141
ACS Appl. Energy Mater. 2018, 1, 5609−5618

(25) Braun, S.; Yada, C.; Latz, A. Thermodynamically Consistent Model for Space-Charge-Layer Formation in a Solid Electrolyte. *J. Phys. Chem. C* **2015**, *119*, 22281−22288.
(26) Landstorfer, M.; Funken, S.; Jacob, T. An Advanced Model Framework for Solid Electrolyte Intercalation Batteries. *Phys. Chem. Chem. Phys.* **2011**, *13*, 12817−12825.
(27) Zimmer, F.; Ballone, P.; Maier, J.; Parrinello, M. Charge Carrier Interactions in Ionic Conductors: A Classical Molecular-Dynamics and Monte Carlo Study on AgI. *J. Chem. Phys.* **2000**, *112*, 6416−6423.
(28) Maier, J. Chemical Potential of Charge Carriers in Solids. *Z. Phys. Chem.* **2005**, *219*, 35−46.
(29) Maier, J. Enhancement of the Ionic Conductivity in Solid-Solid-Dispersions by Surface Induced Defects. *Berich. Bunsengesell.* **1984**, *88*, 1057−1062.
(30) Maier, J. Defect Chemistry and Conductivity Effects in Heterogeneous Solid Electrolytes. *J. Electrochem. Soc.* **1987**, *134*, 1524.
(31) Yamada, H.; Suzuki, K.; Oga, Y.; Saruwatari, I.; Moriguchi, I. Lithium Depletion in the Solid Electrolyte Adjacent to Cathode Materials. *ECS Trans.* **2013**, *50*, 1−12.
(32) Maier, J. Nanoionics: Ion Transport and Electrochemical Storage in Confined Systems. *Nat. Mater.* **2005**, *4*, 805−815.
(33) Zhang, Q.; Pan, J.; Lu, P.; Liu, Z.; Verbrugge, M. W.; Sheldon, B. W.; Cheng, Y. T.; Qi, Y.; Xiao, X. Synergetic Effects of Inorganic Components in Solid Electrolyte Interphase on High Cycle Efficiency of Lithium Ion Batteries. *Nano Lett.* **2016**, *16*, 2011−2016.
(34) Kumar, B.; Nellutla, S.; Thokchom, J. S.; Chen, C. Ionic Conduction through Heterogeneous Solids: Delineation of the Blocking and Space Charge Effects. *J. Power Sources* **2006**, *160*, 1329−1335.
(35) Yamada, H.; Suzuki, K.; Nishio, K.; Takemoto, K.; Isomichi, G.; Moriguchi, I. Interfacial Phenomena between Lithium Ion Conductors and Cathodes. *Solid State Ionics* **2014**, *262*, 879−882.
(36) Maier, J. Ionic Conduction in Space Charge Regions. *Prog. Solid State Chem.* **1995**, *23*, 171−263.
(37) Kim, S.; Fleig, J.; Maier, J. Space Charge Conduction: Simple Analytical Solutions for Ionic and Mixed Conductors and Application to Nanocrystalline Ceria. *Phys. Chem. Chem. Phys.* **2003**, *5*, 2268−2273.
(38) Chen, C. C.; Maier, J. Space Charge Storage in Composites: Thermodynamics. *Phys. Chem. Chem. Phys.* **2017**, *19*, 6379−6396.
(39) Haverkate, L. A.; Chan, W. K.; Mulder, F. M. Large Space-Charge Effects in a Nanostructured Proton Conductor. *Adv. Funct. Mater.* **2010**, *20*, 4107−4116.
(40) Smith, R. B.; Khoo, E.; Bazant, M. Z. Intercalation Kinetics in Multiphase-Layered Materials. *J. Phys. Chem. C* **2017**, *121*, 12505−12523.
(41) Hainovsky, N.; Maier, J. Simple Phenomenological Approach to Premelting and Sublattice Melting in Frenkel Disordered Ionic Crystals. *Phys. Rev. B: Condens. Matter Mater. Phys.* **1995**, *51*, 15789−15797.
(42) Ragavendran, K.; Vasudevan, D.; Veluchamy, A.; Emmanuel, B. Computation of Madelung Energies for Ionic Crystals of Variable Stoichiometries and Mixed Valencies and Their Application in Lithium-Ion Battery Voltage Modeling. *J. Phys. Chem. B* **2004**, *108*, 16899−16903.
(43) Sherwood, D.; Ragavendran, K.; Emmanuel, B. Madelung-Buckingham Model as applied to the Prediction of Voltage, Crystal Volume Changes, and Ordering Phenomena in Spinel-Type Cathodes for Lithium Batteries. *J. Phys. Chem. B* **2005**, *109*, 12791−12794.
(44) Gobel, M. C.; Gregori, G.; Maier, J. Numerical Calculations of Space Charge Layer Effects in Nanocrystalline Ceria. Part I: Comparison with the Analytical Models and Derivation of Improved Analytical Solutions. *Phys. Chem. Chem. Phys.* **2014**, *16*, 10214−10231.
(45) Levi, M. D.; Aurbach, D. Diffusion Coefficients of Lithium Ions during Intercalation into Graphite Derived from the Simultaneous Measurements and Modeling of Electro-chemical Impedance and Potentiostatic Intermittent Titration Characteristics of Thin Graphite Electrodes. *J. Phys. Chem. B* **1997**, *101*, 4641−4647.
(46) Levi, M. D.; Salitra, G.; Markovsky, B.; Teller, H.; Aurbach, D.; Heider, U.; Heider, L. Solid-State Electrochemical Kinetics of Li-Ion Intercalation into $Li_{1-x}CoO_2$: Simultaneous Application of Electroanalytical Techniques SSCV, PITT, and EIS. *J. Electrochem. Soc.* **1999**, *146*, 1279.
(47) Phani Dathar, G. K.; Balachandran, J.; Kent, P. R. C.; Rondinone, A. J.; Ganesh, P. Li-ion Site Disorder Driven Superionic Conductivity in Solid Electrolytes: a First-Principles Investigation of β-Li_3PS_4. *J. Mater. Chem. A* **2017**, *5*, 1153−1159.
(48) Vadlamani, B.; An, K.; Jagannathan, M.; Chandran, K. S. R. An In-Situ Electrochemical Cell for Neutron Diffraction Studies of Phase Transitions in Small Volume Electrodes of Li-Ion Batteries. *J. Electrochem. Soc.* **2014**, *161*, A1731−A1741.
(49) Arbi, K.; Hoelzel, M.; Kuhn, A.; Garcia-Alvarado, F.; Sanz, J. Structural Factors that Enhance Lithium Mobility in Fast-Ion $Li_{(1+x)}Ti_{(2-x)}Al_x(PO_4)_3$ ($0 \le x \le 0.4$) Conductors Investigated by Neutron Diffraction in the Temperature Range 100−500 K. *Inorg. Chem.* **2013**, *52*, 9290−9296.
(50) Buschmann, H.; Dolle, J.; Berendts, S.; Kuhn, A.; Bottke, P.; Wilkening, M.; Heitjans, P.; Senyshyn, A.; Ehrenberg, H.; Lotnyk, A.; Duppel, V.; Kienle, L.; Janek, J. Structure and Dynamics of the Fast Lithium Ion Conductor $Li_7La_3Zr_2O_{12}$. *Phys. Chem. Chem. Phys.* **2011**, *13*, 19378−19392.
(51) Choi, Y.-M.; Pyun, S.-I.; Bae, J.-S.; Moon, S.-I. Effects of Lithium Content on the Electrochemical Lithium Intercalation Reaction into $LiNiO_2$ and $LiCoO_2$ Electrodes. *J. Power Sources* **1995**, *56*, 25−30.
(52) Nanjundaswamy, K. S.; Padhi, A. K.; Goodenough, J. B.; Okada, S.; Ohtsuka, H.; Arai, H.; Yamaki, J. Synthesis, Redox Potential Evaluation and Electrochemical Characteristics of NASICON Related 3D Framework Compounds. *Solid State Ionics* **1996**, *92*, 1−10.
(53) Lv, S.; Li, Z.; Li, Z.; Ganapathy, S.; van Eck, E. R. H.; Wagemaker, M. The Garnet Structure-Ionic Liquid Composite Electrolyte for Li-ions Conducting Paths Interconnecting the Double Layers. Unpublished work in preparation.
(54) Rao, K. V.; Smakula, A. Dielectric Properties of Cobalt Oxide, Nickel Oxide, and Their Mixed Crystals. *J. Appl. Phys.* **1965**, *36*, 2031−2038.
(55) Delhaes, P.; Manceau, J. P.; Guerard, D. Physical Properties of First and Second Stage Lithium Graphite Intercalation Compounds. *Synth. Met.* **1980**, *2*, 277−284.
(56) Zangina, T.; Hassan, J.; Matori, K. A.; Azis, R. S.; Ahmadu, U.; See, A. Sintering Behavior, AC Conductivity and Dielectric Relaxation of $Li_{1.3}Ti_{1.7}Al_{0.3}(PO_4)_3$ NASICON Compound. *Res. Phys.* **2016**, *6*, 719−725.
(57) Rettenwander, D.; Welzl, A.; Cheng, L.; Fleig, J.; Musso, M.; Suard, E.; Doeff, M. M.; Redhammer, G. J.; Amthauer, G. Synthesis, Crystal Chemistry, and Electrochemical Properties of $Li_{(7-2x)}La_3Zr_{(2-x)}Mo_xO_{12}$ (x = 0.1−0.4): Stabilization of the Cubic Garnet Polymorph via Substitution of Zr(4+) by Mo(6+). *Inorg. Chem.* **2015**, *54*, 10440−9.
(58) Wachter-Welzl, A.; Wagner, R.; Rettenwander, D.; Taibl, S.; Amthauer, G.; Fleig, J. Microelectrodes for Local Conductivity and Degradation Measurements on Al Stabilized $Li_7La_3Zr_2O_{12}$ Garnets. *J. Electroceram.* **2017**, *38*, 176−181.
(59) Wolverton, C.; Zunger, A. First-Principles Prediction of Vacancy Order-Disorder and Intercalation Battery Voltages in Li_xCoO_2. *Phys. Rev. Lett.* **1998**, *81*, 606−609.
(60) Yokokawa, H. Thermodynamic Stability of Sulfide Electrolyte/Oxide Electrode Interface in Solid-State Lithium Batteries. *Solid State Ionics* **2016**, *285*, 126−135.
(61) Setton, R.; Conard, J. Madelung Energy and Stability of the Compound Li_7C_{24} Prepared Under Pressure. *Mol. Cryst. Liq. Cryst. Sci. Technol., Sect. A* **1994**, *244*, 307−312.
(62) Il'ina, E. A.; Raskovalov, A. A.; Safronov, A. P. The Standard Enthalpy of Formation of Superionic Solid Electrolyte $Li_7La_3Zr_2O_{12}$. *Thermochim. Acta* **2017**, *657*, 26−30.

DOI: 10.1021/acsaem.8b01141
ACS Appl. Energy Mater. 2018, 1, 5609−5618

(63) Epp, V.; Ma, Q.; Hammer, E. M.; Tietz, F.; Wilkening, M. Very Fast Bulk Li Ion Diffusivity in Crystalline $Li_{1.5}Al_{0.5}Ti_{1.5}(PO_4)_3$ as seen using NMR Relaxometry. *Phys. Chem. Chem. Phys.* **2015**, *17*, 32115−32121.
(64) O'Neill, H.; Navrotsky, A. Simple Spinels: Crystallographic Parameters, Cation Radii, Lattice Energies, and Cation Distribution. *Am. Mineral.* **1983**, *68*, 181−194.
(65) Thomas, M.; Bruce, P.; Goodenough, J. B. AC Impedance Analysis of Polycrystalline Insertion Electrodes: Application to $Li_{1-x}CoO_2$. *J. Electrochem. Soc.* **1985**, *132*, 1521.
(66) Kozinsky, B.; Akhade, S. A.; Hirel, P.; Hashibon, A.; Elsasser, C.; Mehta, P.; Logeat, A.; Eisele, U. Effects of Sublattice Symmetry and Frustration on Ionic Transport in Garnet Solid Electrolytes. *Phys. Rev. Lett.* **2016**, *116*, No. 055901.
(67) Han, F.; Zhu, Y.; He, X.; Mo, Y.; Wang, C. Electrochemical Stability of $Li_{10}GeP_2S_{12}$ and $Li_7La_3Zr_2O_{12}$ Solid Electrolytes. *Adv. Ener. Mater.* **2016**, *6*, 1501590.
(68) Wenzel, S.; Randau, S.; Leichtweiss, T.; Weber, D.; Sann, J.; Zeier, W.; Janek, J. Direct Observation of the Interfacial Instability of the Fast Ionic Conductor $Li_{10}GeP_2S_{12}$ at the Lithium Metal Anode. *Chem. Mater.* **2016**, *28*, 2400−2407.
(69) Wenzel, S.; Sedlmaier, S.; Dietrich, C.; Zeier, W.; Janek, J. Interfacial Reactivity and Interphase Growth of Argyrodite Solid Electrolytes at Lithium Metal Electrodes. *Solid State Ionics* **2018**, *318*, 102.
(70) Han, F.; Gao, T.; Zhu, Y.; Gaskell, K. J.; Wang, C. A Battery Made from a Single Material. *Adv. Mater.* **2015**, *27*, 3473−83.
(71) Haruyama, J.; Sodeyama, K.; Han, L. Y.; Takada, K.; Tateyama, Y. Space-Charge Layer Effect at Interface between Oxide Cathode and Sulfide Electrolyte in All-Solid-State Lithium-Ion Battery. *Chem. Mater.* **2014**, *26*, 4248−4255.

DOI: 10.1021/acsaem.8b01141
ACS Appl. Energy Mater. 2018, 1, 5609−5618